Metal-binding processes on Nanoplastics : Rare earth elements as a probe

Florent Blancho, Mélanie Davranche, Remi Marsac, Adrien Leon, Aline Dia, Bruno Grassl, Stephanie Reynaud, Julien Gigault

Environmental Science Nano

Accepted Manuscript

This article can be cited before page numbers have been issued, to do this please use: F. Blancho, M. Davranche, R. Marsac, A. Leon, A. Dia, B. Grassl, S. Reynaud and J. Gigault, *Environ. Sci.: Nano*, 2022, DOI: 10.1039/D2EN00048B.

ROYAL SOCIETY OF CHEMISTRY

rsc.li/es-nano

View Article Online
DOI: 10.1039/D2EN00048B

Environmental Significance Statement

Due to their colloidal properties, nanoplastics could influence trace metal speciation in natural matrices, which has been poorly addressed due to the lack of methodology to assess the nanoplastics -metal association in the natural environment. To give a global picture of this property for nanoplastics, this work aims at using rare earth elements (REE) as a chemical probe to understand metal adsorption mechanisms that could occur onto nanoplastics surfaces. We demonstrated that the denticity of the complexes is influenced by the pH and competitive ions. This study is a novel approach in understanding NPs-metals interaction and highlights REE as a powerful tracer of sorption mechanisms.

View Article Online
DOI: 10.1039/D2EN00048B

Metals binding processes on Nanoplastics : Rare earth elements as a probe

Florent Blancho[1], Mélanie Davranche[1], Rémi Marsac[1], Adrien Léon[1], Aline Dia[1], Bruno Grassl[2], Stéphanie[2] Reynaud, and Julien Gigault[1,3],*

[1]Laboratoire Géosciences Rennes, UMR6118, 263 Avenue Général Leclerc, 35042 Rennes

[2.] IPREM, CNRS / Université de Pau et des Pays de L'Adour, F64000 Pau, France

[3] TAKUVIK laboratoy, UMI3376 CNRS/Université Laval, Québec, Canada

E-mail contact: julien gigault@takuvik.ulaval.ca

Keywords:

Nanoplastics; Sorption; Metals; Characterization; Rare earth elements

View Article Online
DOI: 10.1039/D2EN00048B

Abstract

The nanoplastics presence in the ocean and soil demonstrates their global distribution in the environment. Due to their colloidal properties, nanoplastics could influence trace metal speciation in natural matrices, which has been poorly addressed due to the lack of methodology to assess the nanoplastics -metal association in the natural environment. To give a global picture of this property for nanoplastics, this work aims at using rare earth elements (REE) as a chemical probe to understand metal adsorption mechanisms that could occur onto nanoplastics surfaces, which is expected to be highly oxidized in the environment. Comparison between environmentally relevant nanoplastics' models and REE-COOH complexes patterns demonstrated that REE are adsorbed through the COOH sites onto the nanoplastics. These adsorptions pathways follow a mono-ligand process for light REE and bi-ligand for heavy REE complexes, chelate being excluded. We demonstrated that the denticity of the complexes is influenced by the pH, REE loading, and competitive ions. Bi-ligand complexes with heavy REE dominate at pH>4.5 and low REE loading. This study is a novel approach in understanding NPs-metals interaction and highlights REE as a powerful tracer of sorption mechanisms.

View Article Online
DOI: 10.1039/D2EN00048B

Introduction

The presence of nanoplastics (NPs) in various environmental compartments, notably ocean, soils, and alpine snows, is now evidenced (1–3). When released in the environment, plastics waste fragments into plastic particles of various sizes, mainly through mechanical abrasion and photo/thermo-oxidation (4–7). Nanoplastics are particles < 1000 nm with heterogeneous shapes and charged surfaces (8). Nanoplastics act as colloids, and regarding their nanometric size, they are expected to have larger specific surface area (SSA) than microplastics resulting in an enhancing of their surface reactivity for micropollutants (7,9–12). Recent ecotoxicological studies showed the release of organic and inorganic pollutants associated with NPs in living organisms, namely the "trojan horse effect" (13–15).

However, information and data are scarce for inorganic pollutants, notably metal interactions with NPs. Nevertheless, metals are used mainly in the plastic formulation as color pigments or provide specific properties to plastics (16,17). These metals are trapped in the polymer structure. Although their diffusion within plastic polymer bodies is possible, this process is slow and expects to release very few amounts of metal (17–19). However, when plastics are photodegraded and subsequently fragmented as micro-and nanoplastics, their metal loading is also released. Catrouillet et al. (20) showed that most metal adsorbed on the altered surface layers of microplastics came from the metals additives used to form the plastic. Since this altered layer is also the source of NPs released in the environment, it can be hypothesized that metal and NPs interact from their release.

Moreover, it is not excluded that metal is initially present in the environment (such as in landfills), and NPs can interact independently of their release. Davranche et al. (10) demonstrated that Pb(II) is associated with NPs principally by surface complexation and intraparticle diffusion. However, this study focused only on the Pb(II) uptake and did not evaluate the sorption mechanisms. At the same time, ATR-FTIR and XPS analysis evidenced that O-containing functions (21–23) and carboxylic sites are present on the surface of NPs and the altered surface of microplastics sampled in the environment

View Article Online
DOI: 10.1039/D2EN00048B

(24,25). Tang et al. [23] suggested that –COOH is the principal functional group at the MPs surface associated with metals. And yet, compared to microplastics, it was demonstrated that the NPs reactive surface site density could reach 11 sites nm^{-2}, higher than goethite (24,26,27). It is, therefore, crucial to determine how NPs properties could affect the fate and behavior of trace metals.

Several techniques exist to characterize the complexes formed between metals and solids. One of the most resolved is the X-ray absorption (XAS, etc.), which was successfully used to investigate the metal complexation by minerals and colloids (26,28–30). But such a technique is challenging to operate for accurate determination of the speciation. One interesting strategy is to use geochemical proxies as a probe for sorption studies. Rare earth elements (REE) represent a group of chemical elements with coherent chemical properties that allow their use as a fingerprint of sources and biogeochemical processes (31–36). Their chemical properties present systematic changes along with the range of their atomic number, resulting in typical distribution patterns (37). For natural organic matter (OM), REE patterns have successfully described the metal-binding mechanisms. They are notably sensitive to the number of chemical bindings or ligands surrounding REE and can therefore provide information on the complex denticity (38–40).

This work aims at evaluating the ability of REE to determine the adsorption mechanism of trace metals occurring at the NPs' surface. Rare earth elements were used as a probe to characterize the NPs functional groups that control the sorption and complexes formed between metal and NPs. Rare earth elements adsorption isotherm and pH-adsorption edge were performed with REE and three NPs models, 1) the commonly used carboxylate polystyrene nano-beads including surfactant ($PSL_{surfactant}$), 2) carboxylate polystyrene nano-beads without surfactant (PSL_{free}) from Pessoni et al, 2019 (41), and 3) an environmentally-relevant NPs produced following Blancho et al., 2021 (24). Experimental REE patterns were compared to literature REE ligands patterns to decipher the occurring mechanisms.

View Article Online
DOI: 10.1039/D2EN00048B

Materials and methods

Nanoplastics models

Nanoplastics models were 200 nm, carboxylate polystyrene Latex nanoparticles (Polysciences Europe), $PSL_{surfactant}$, 380 nm free soap Polystyrene latex nanoparticles, PSL_{free} (41). The e-NPs model is an environmentally-relevant NPs, produced from highly altered plastics debris collected at the surface from the Nord Pacific Garbage patch. They are produced following the Blancho et al. 2021 protocol (24). The three NPs size were obtained from Dynamic Light Scattering (DLS) measurement. Theirsurface specific area was quantified by BET (Brunnauer Emmet et Teller). The density of the ionizable group was determined from potentiometric titration. Theused methodology are described in the supplementary file (SI. 1).

The NPs suspensions was quantified using theircarbon content by measuring the total organic carbon (TOC) (TOC-V analyzer, Shimadzu). The concentration of NPs are thus given in mg Carbon L^{-1}. The precision of the TOC measurements was estimated to be ± 5% using a standard potassium hydrogen phthalate solution (Sigma Aldrich).

Adsorption experiments

Adsorption isotherms of REE by NPs were carried out for REE/NPs ratios from 0.025 to 1 mg g^{-1} Carbon in triplicates. The stock solution of REE was the REE standard CCS-1 solution (Inorganic Venture) that contained equal concentrations of REE, Sc, U, Th, and Y. The concentration of NPs was fixed at 50 and 25 ppm for both PSLs and the e-NPs, respectively, regarding the low amount of produced e-NPs. The ionic strength (IS) was fixed at 5 mM with $NaNO_3$ (Fisher Scientific). After adding REE, the pH of the suspension was adjusted to 5 with HNO_3 and/or NaOH (0.1 to 1 mol L^{-1}). At equilibrium, the suspensions were filtered at 0.2 µm (PES syringe filter, Sartorius) for both PSLs and 30 kD for e-NPs (PES ultrafiltration cells, Sartorius). The equilibrium time was estimated from previous kinetic experiments to 48h for all NPs. Dynamic light scattering previously checked the

View Article Online
DOI: 10.1039/D2EN00048B

absence of nanoparticles in the filtrate (VASCO Flex, Cordouan Technologies). After filtration, all samples were acidified at 2% HNO_3 for ICP-MS analysis.

The pH-adsorption edge experiments were carried out in triplicates, with REE concentration at 0.1 and 0.35 mg g C^{-1} for both PSLs and e-NPs, respectively. The pH was fixed at pH 3, 4.5, 5, 5.5, 6, and 7 with HNO_3 or NaOH. At equilibrium, the suspensions were filtered at 0.2 µm (PES, Sartorius) for both PSLs and 30 kDa for e-NPs (PES ultrafiltration cells, Sartorius). After filtration, all samples were acidified at 2% HNO_3 for ICP-MS measurements.

REE Analysis

The REE concentrations were measured using a Quadrupole ICP-MS (Agilent Technologies 7700X). Before metal quantification, calibration curves were performed and validated using certified material references (SLRS-6, National Research Council). A rhodium solution was used as an internal standard to correct the instrumental drift and potential matrix effects. The average limit of REE quantification was determined at 0.4 ± 0.02 ppt (AFNOR Certification). Moreover, as the upper limit of the REE calibration curve was 5 ppb, if necessary, samples were diluted not to exceed this value. Chemical blanks were consistently below the limit of quantification and were thus neglected.

Results and discussion

PSL with surfactant

Adsorption isotherms showed that $[REE]_{ads}$ increased with the increasing $[REE]_{free}$ to reach a strict asymptotic plateau indicating a surface site saturation (Figure 1A). The maximum adsorption concentrations were 0.06 and 0.13 mg g^{-1} C for La, Eu, and Lu. The adsorption increased thus from La, Eu to Lu demonstrating that light REE (LREE) are lesser adsorbed at the $PSL_{surfactant}$ surface than the middle (MREE) or heavy REE (HREE). The isotherm shape did not vary, suggesting a similar adsorption mechanism for all REE. The corresponding REE-NPs binding patterns exhibited an MREE

View Article Online
DOI: 10.1039/D2EN00048B

downward concavity supported by the La/Sm ratio variations (from 0.93 at REE/NPs = 0.025 to 0.9 from REE/NPs = 1, SI. 2). This feature is specific to the REE binding by carboxylic groups –COOH (33,34,38,42,43) (Figure 1B) and was expected for the $PSL_{surfactant}$ since carboxylated. The La/Lu ratios varied regularly from 0.94 to 0.89. The increasing REE/NPs ratios suggested a slight HREE adsorption increase than the other REE, increasing REE/NPs ratios (SI. 2).

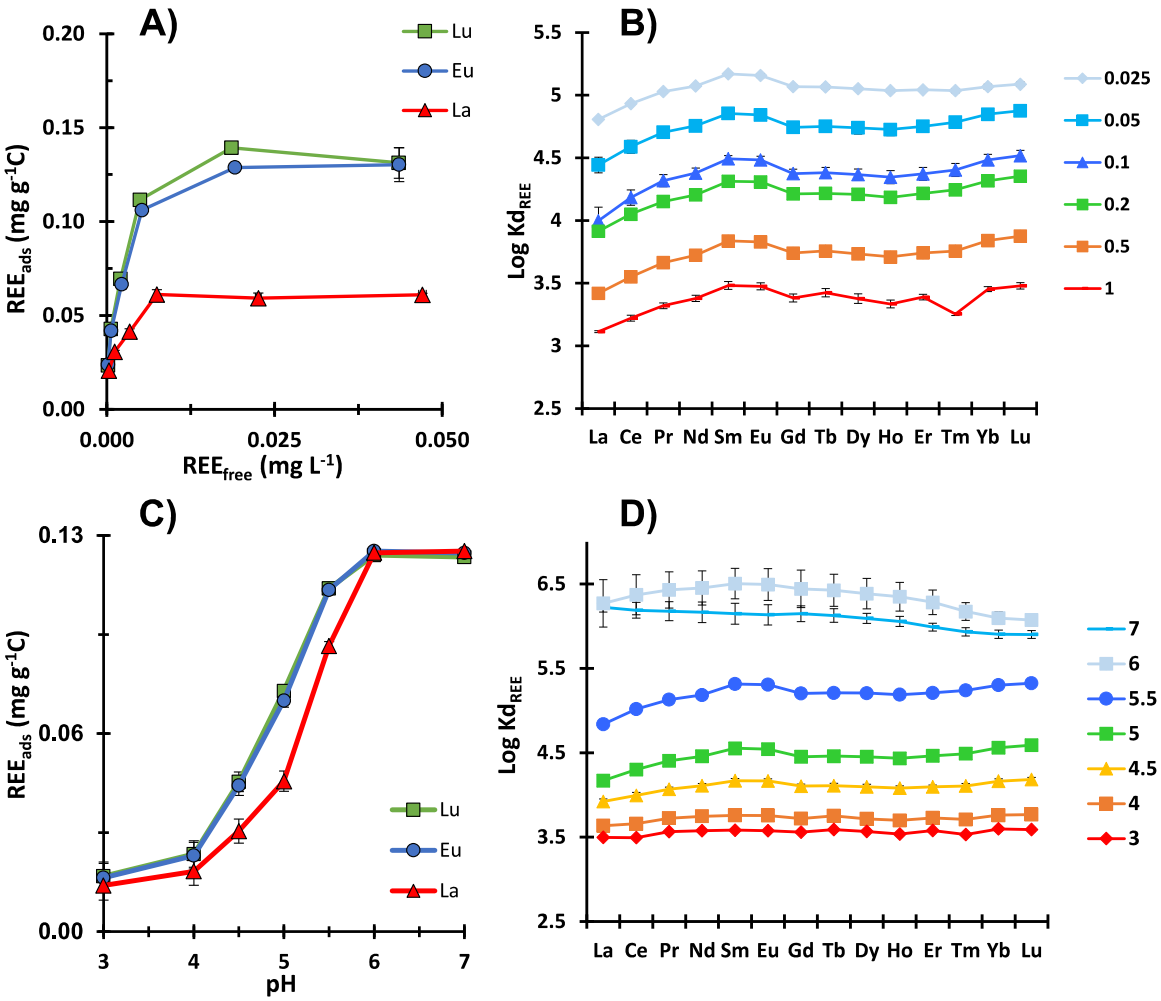

Figure 1. A) Adsorption isotherm of REE onto $PSL_{surfactant}$ for REE/NPs varying from 0.05 to 1 and pH = 6.5, B) REE patterns (log Kd) corresponding to each point of the adsorption isotherm, C) REE adsorption relative to the pH at REE/NPs = 0.1 mg g^{-1} for pH varying from 3 to 7, D) REE patterns (log Kd) corresponding to each point of the pH-adsorption-edge. Error bars correspond to the SD of the triplicates.

View Article Online
DOI: 10.1039/D2EN00048B

Figure 1C illustrates adsorbed La, Eu, and Lu relative to pH. It shows that the adsorption process was strongly dependent on pH. Adsorption thus occurred through ionizable binding sites. Except for near-total adsorption from pH 6, adsorption decreased from Eu>Lu>La, MREE being the most adsorbed REE. The corresponding REE patterns were flat at low pH, not enough REEs were adsorbed to obtain a significant REE fractionation (La/Lu= 0.97 and La/Sm= 0.97 at pH 3, SI. 2) (Figure 1D). At intermediary pH, an MREE downward concavity (La/Sm = 0.94 to 0.91 between pH 4 to 5.5) and a small HREE adsorption increase (La/Lu= 0.94 to 0.91 between pH 4 to 5.5, SI. 2) were observed on the REE patterns. The MREE enrichment resulted from the preferential MREE binding to the –COOH groups. REE patterns were flatter at high pH, decreasing from La to Lu (La/Lu = 1.05 at pH 7, SI. 2). In such a pH condition, around 99.99 % of REE were adsorbed, and fractionations between REE were small, except for HREE partly maintained in solution by carbonate from pH 6.

PSL without surfactant, PSL_{free}

For PSL free, adsorption isotherm showed that $[REE]_{ads}$ increased with the $[REE]_{free}$ until $[La]_{ads}$ = 0.04 mg g^{-1} C at $[La]_{free}$ ≈0.003 mg L^{-1}, $[Eu]_{ads}$ = 0.1 mg g^{-1} C at $[Eu]_{free}$ ≈0.013 mg L^{-1} and $[Lu]_{ads}$ = 0.08 mg g^{-1} C at $[Lu]_{free}$ ≈0.014 mg L^{-1} (Figure 2A). Adsorption was lower than $PSL_{surfactant}$ due to PSL_{free} lower site density, 2.8 sites nm^{-2} against 5.7 sites nm^{-2} for $PSL_{surfactant}$ (SI. 1). Adsorption was higher for Eu>Lu>La. Middle REEs were thus the most adsorbed. The $[REE]_{ads}$ decreased without reaching any plateau. No site saturation occurred. The $[REE]_{ads}$ decrease occurred in response to the REE competition with Y, U, Sc, Th, which are simultaneously present in the stock solution used to perform the adsorption experiments. This competition occurred for the PSL_{free} due to its small surface site density (SI. 1). This competition had a higher impact on La than on Lu and Eu adsorption since occurring from $[La]_{free}$ ≈0.003 mg L^{-1} against 0.013 mg L^{-1} and 0.014 mg L^{-1} for Eu and Lu, respectively. As for carboxylated $PSL_{surfactant}$, REE-NPs binding patterns exhibit an MREE downward concavity specific to the REE binding with carboxylic groups (Figure 2B). Moreover, the La/Lu and

View Article Online
DOI: 10.1039/D2EN00048B

the La/Sm ratio decreased continuously from 0.97 to 0.84 and 0.91 to 0.79, respectively, with the increasing REE/NPs suggesting a regular depletion of La (SI. 2, Figure 2B). This decrease might be explained by the increasing competition between the LREE and Y, U, Sc, and Th for the PSL_{free} binding sites with the increasing elements loading onto PSL_{free}.

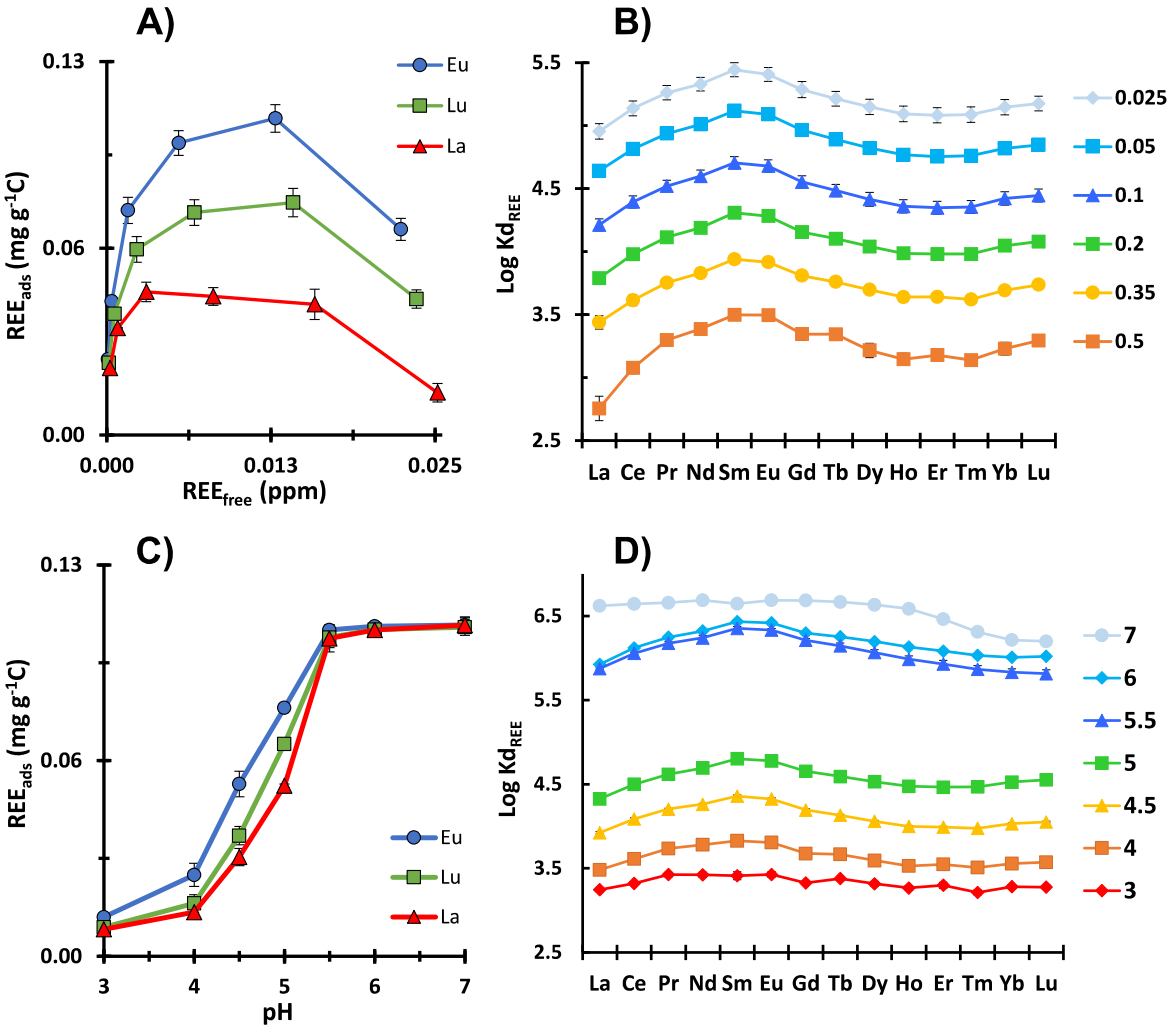

Figure 2. A) Adsorption isotherm of REE onto PSL_{free} for REE/NPs varying from 0.05 to 1 and pH = 6.5, B) REE patterns (log Kd) corresponding to each point of the adsorption isotherm, C) REE adsorption relative to the pH at REE/NPs = 0.1 mg g^{-1} for pH varying from 3 to 7, D) REE patterns (log Kd) corresponding to each point of the pH-adsorption-edge. Error bars correspond to the SD of the triplicates.

View Article Online
DOI: 10.1039/D2EN00048B

Adsorption of La, Eu, and Lu relative to pH was plotted in figure 2C. The $[REE]_{ads}$ increased with the increasing pH, indicating adsorption occurred via ionizable binding sites. Adsorption decreased from Eu>Lu>La, MREE being the most adsorbed. Not enough REEs were adsorbed at low pH to obtain a significant REE fractionation (Figure 2D). At intermediary pH, an MREE downward concavity was developed (La/Sm = 0.92 and 0.90 at pH 3 and 5, respectively, SI. 2). The MREE enrichment resulted from the preferential MREE binding to the –COOH groups. The La/Lu ratio decreased from 0.97 to 0.95 between pH 3 to 5 until reaching 1.1 at pH 7, suggesting a slight HREE enrichment at intermediary pHs (SI. 2). By contrast, at pH 7, the REE pattern was depleted in HREE in response to HREE preferential complexation by carbonate in solution.

Environmentally relevant, e-NPS

For e-NPs, $[REE]_{ads}$ continuously increased with the $[REE]_{free}$, no plateau, namely site saturation, was reached, suggesting a heterogeneous adsorption process relative to the REE/NPs ratios (Figure 3A). The adsorbed amount of all REEs was higher than for both PSLs, while the adsorption followed the same order, Eu>Lu> La, indicating that MREE were the most adsorbed. This higher adsorption, as well as the heterogeneous adsorption process, could be the result of the higher site density of the e-NPs ($\geq$14.2 sites nm^{-2}, SI. 1) as compared to both PSLs (5.7 and 2.8 sites nm^{-2} for $PSL_{surfactant}$ and PSL_{free}, respectively, SI. 1). This highest site density allowed more REE adsorb and probably formed different complexes. The corresponding REE patterns exhibited the highest log Kd at high REE/NPs ratios than PSL (Figure 3B). The La/Sm ratios varied from 0.95 to 0.97 in response to developing an MREE downward concavity corresponding to the REE binding to –COOH sites (SI. 2). However, by contrast with both PSLs, the La/Sm ratio increased with the decreasing ratio (SI. 2). This result can be due to both La adsorption decreases or Sm adsorption increase, namely an MREE downward concavity variation. The La/Lu ratios also continuously increased from 0.95 to 0.99, with the decreasing

View Article Online
DOI: 10.1039/D2EN00048B

REE/NPs ratios indicating an increase of the HREE adsorption or a decrease of the LREE adsorption (SI. 2).

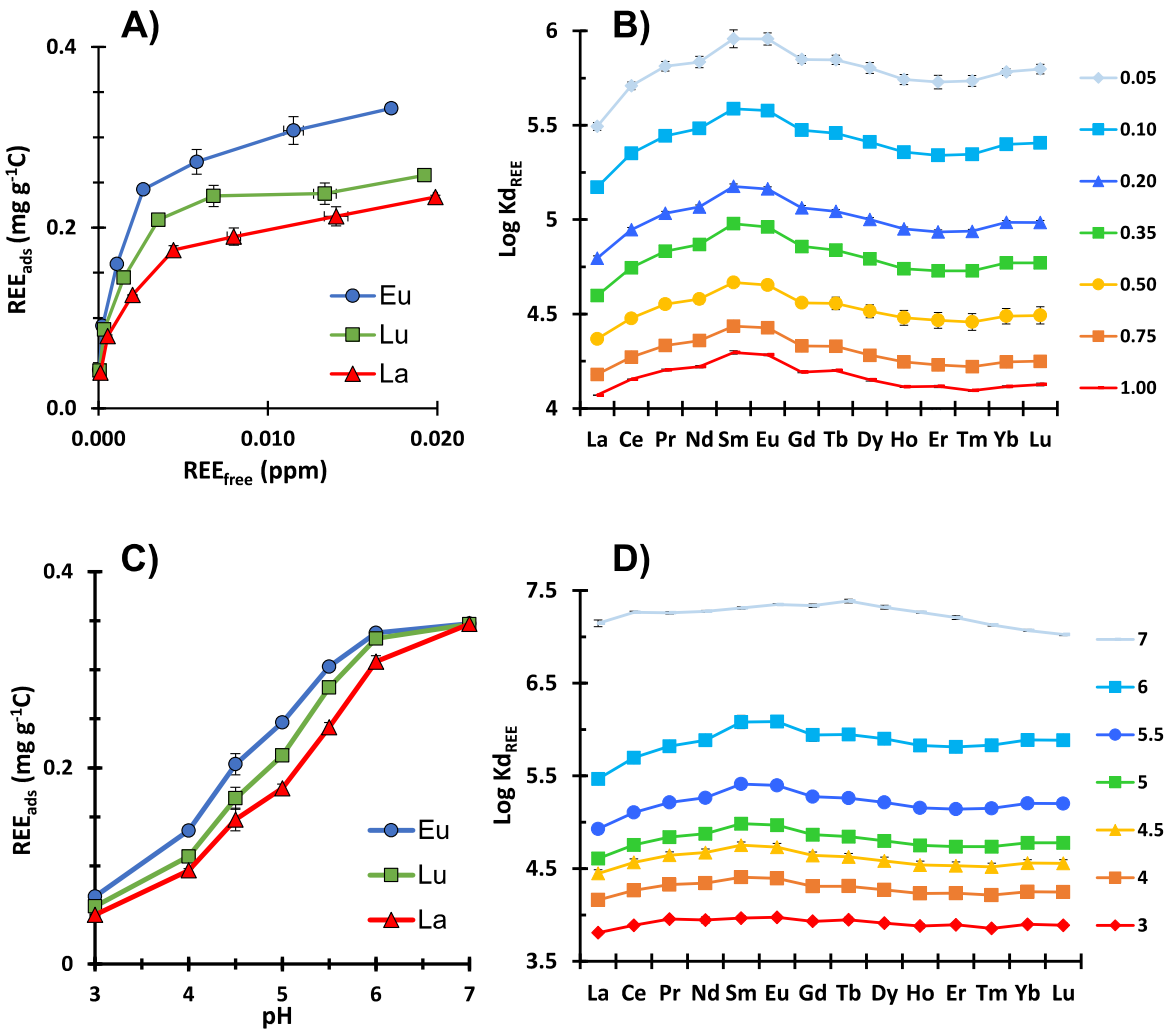

Figure 3. A) Adsorption isotherm of REE onto e-NPs for REE/NPs varying from 0.05 to 1 and pH = 6.5, B) REE patterns (log Kd) corresponding to each point of the adsorption isotherm, C) REE adsorption relative to the pH at REE/NPs = 0.35 mg g^{-1} for pH varying from 3 to 7, D) REE patterns (log Kd) corresponding to each point of the pH-adsorption-edge. Error bars correspond to the SD of the triplicates

The [REE]$_{ads}$ increased with the increasing pH (Figure 3C). The adsorption was thus pH-dependent and occurred onto ionizable sites. The amount of adsorbed REE was higher than for both PSLs, not only for each pH but also relative to the pH, notably at lower pHs. At pH =4, 3.6% of REE were adsorbed for e-NPs against 0.4% and 0.2 % for PSL$_{surfactant}$ and PSL$_{free}$, respectively. These results suggest that binding

View Article Online
DOI: 10.1039/D2EN00048B

sites of the highest energy existed, and strong complexes were formed at the surface of the e-NPs. For the corresponding REE-NPs binding patterns, the La/Sm ratios continuously decreased until pH 6, developing an MREE downward concavity. The La/Lu ratios also decreased with the pH increase due to the HREE's higher adsorption (SI. 2). From pH 6.5, both ratios were close to 1, indicating a flat REE pattern and showing that e-NPs were more competitive to carbonate than both PSLs towards REE complexation.

These results suggest that e-NPs are the strongest adsorbent than both PSLs, which have binding sites of various energy and/or can form different complexes with REE and compete with carbonate for REE binding.

REE pattern deciphering

To obtain more information on the REE-NPs complexes, the present REE patterns were compared to the REE patterns binding with various –COOH ligands. The impact of the denticity and the ligand numbers were also compared to obtain information on the complex formed onto the NPs surface.

View Article Online
DOI: 10.1039/D2EN00048B

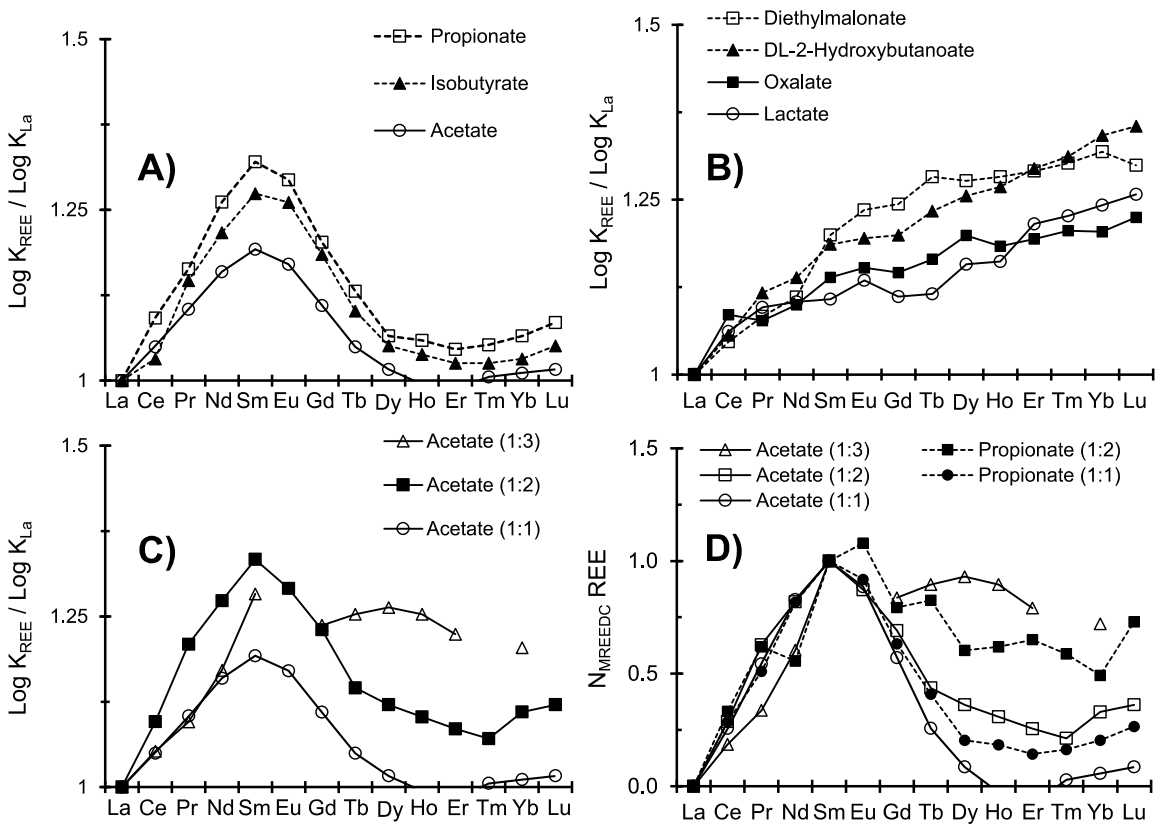

Figure 4. Log K_{REE} patterns normalized to log K_{La} for A) monocarboxylic acids (1:1), B) for REE monodentate complexes with oxo carboxylic and dicarboxylic acid, C) for 1:1, 1:2, and 1:3 REE-acetate complexes, and D) N_{MREEDC} REE patterns of REE-acetate, 1:1, 1:2, 1:3 complexes and REE-propionate 1:1, 1:2 complexes (see SI 3. For references).

Patterns exhibit an increasing MREE downward concavity with the increasing ligands number (Figure 4C). For mono-ligands and multi-ligands complexes between REE and carboxylates (i.e., acetate and propionate), log K patterns exhibit an MREE downward concavity with a maximum binding for Sm as a slight HREE increase, as observed for the experimental REE patterns (Figure 4A). Log K patterns for chelates formed between REE and dicarboxylic (oxalate, diethyl malonate, etc.) or hydroxycarboxylic ligands (i.e., lactate, hydroxybutanoate) exhibit an enrichment from La to Lu (Figure 4B) but no significant MREE downward concavity by contrast with the experimental REE-NPs patterns, avoiding the potential formation of chelate complexes between REE and all NPs models. Experimental REE patterns were thus only compared to the REE patterns of 1:1, 1:2, and 1:3 REE-COOH ligands, namely

View Article Online
DOI: 10.1039/D2EN00048B

acetate and propionate. However, as previously shown from the experimental datasets, state on a potential HREE increase/decrease on the REE patterns is not trivial regarding the variation of the MREE downward concavity. The same remark can be made for the REE-acetate and REE-propionate patterns. To counter this effect, the REE patterns were normalized to the MREE downward concavity as:

$$N_{MREEDC}\,REE = \log (REE/La) / \log (Sm/La)$$

This normalization (N_{MREEDC}) allowed us to observe an increase of the HREE compared to the other REE with the ligand numbers on the REE patterns (Figure 4D).

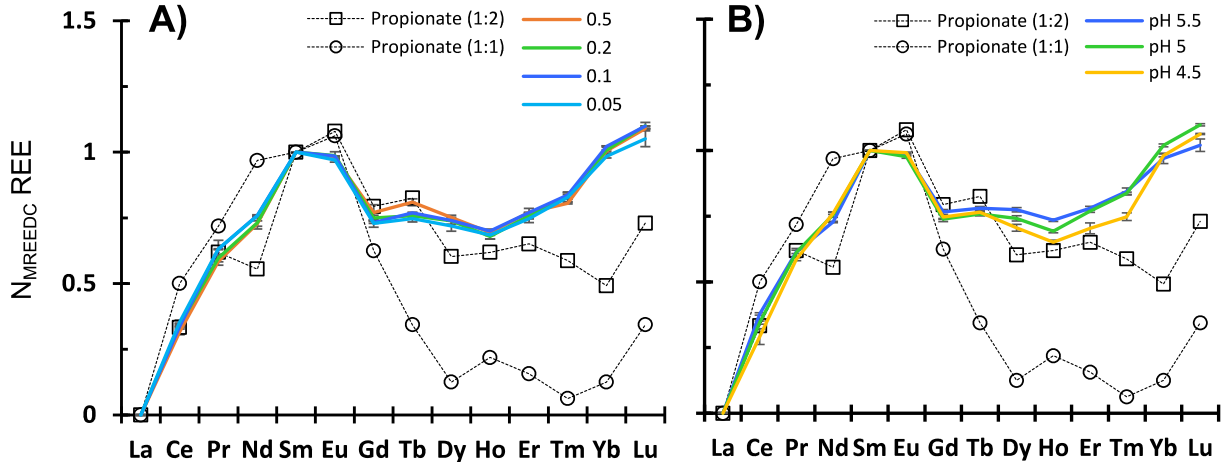

Figure 5. Comparison of REE-$PSL_{surfactant}$ patterns normalized to the MREE downward concavity A) relative to the REE/NPs ratios in mg g^{-1} C and B) relative to pH with the 1:1 and 1:3 REE-propionate complexes patterns normalized to the MREE downward concavity. Error bars correspond to the SD of the triplicates

For $PSL_{surfactant}$, the N_{MREEDC} normalized REE patterns did not evolve with the REE/NPs ratios or pH (Figure 5). Moreover, experimental REE patterns were close in shape to that of the REE-Propionate 1:2 complex suggesting the formation of bi-ligand complexes between REE and 2 –COOH surface sites of the $PSL_{surfactant.}$ This bi-ligand complex predominated as no significant variations of the HREE adsorption were observed.

View Article Online
DOI: 10.1039/D2EN00048B

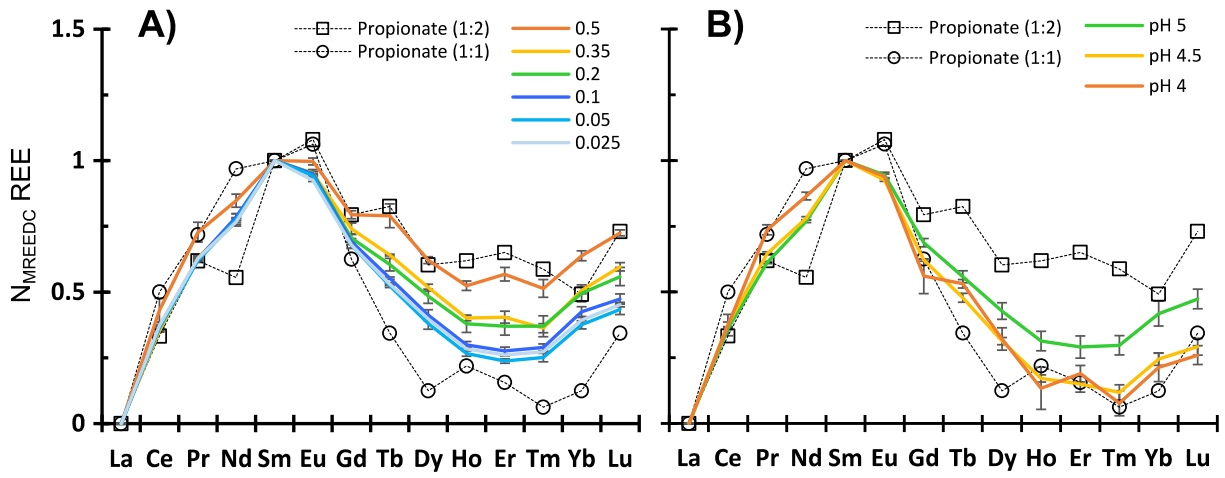

Figure 6. Comparison of REE-PSL_{free} patterns normalized to the MREE downward concavity A) relative to the REE/NPs ratios in mg g^{-1} C and B) relative to pH with the 1:1 and 1:3 REE-propionate complexes patterns normalized to the MREE downward concavity. Error bars correspond to the SD of the triplicates.

For the PSL_{free}, the N_{MREEDC} REE patterns exhibited an increase of HREE with the REE/NPs ratios up to 0.5 mg g^{-1}C (Figure 6A). The N_{MREEDC} REE patterns were comprised between the 1:1 and 1.2 REE-propionate complexes, suggesting an evolution of the binding number and the complexes formed between HREE and PSL_{free}. A simple comparison of the normalized patterns suggested that mono-ligand complexes were formed at low REE/NPs ratios (low REE loading) although the high availability of the binding site. By contrast, bi-ligand complexes were formed at high REE/NPs ratios (high REE loading) although with lower availability of the binding site. Relative to the pH, normalized REE patterns showed that the pH increases also promoted the formation of bi-ligand complexes in response to the deprotonated sites' increasing availability. Both results were incoherent and antagonist. Variations of the REE pattern did not correspond to an HREE adsorption increase but an LREE adsorption decrease (Figure 2A and B). At high REE/NPs ratios, adsorption isotherms and REE patterns showed that competition with Y, U, Sc, and Th was more pronounced for LREE than for HREE (Figure 2 A and B). Detailed observation of the REE patterns variation with the REE/NPS ratio clearly showed an LREE decrease at high REE/NPs ratios (Figure 2B). Therefore, the REE pattern variation can be interpreted as forming strong bi-ligand complexes for HREE that limit competition. At

View Article Online
DOI: 10.1039/D2EN00048B

the same time, LREE formed weak mono-ligand complexes unable to maintain the LREE at the PSL_{free} surface. This process can be observed here because of the low site's density of the PSL_{free} and the resulting competition with Y, U, Sc, and Th.

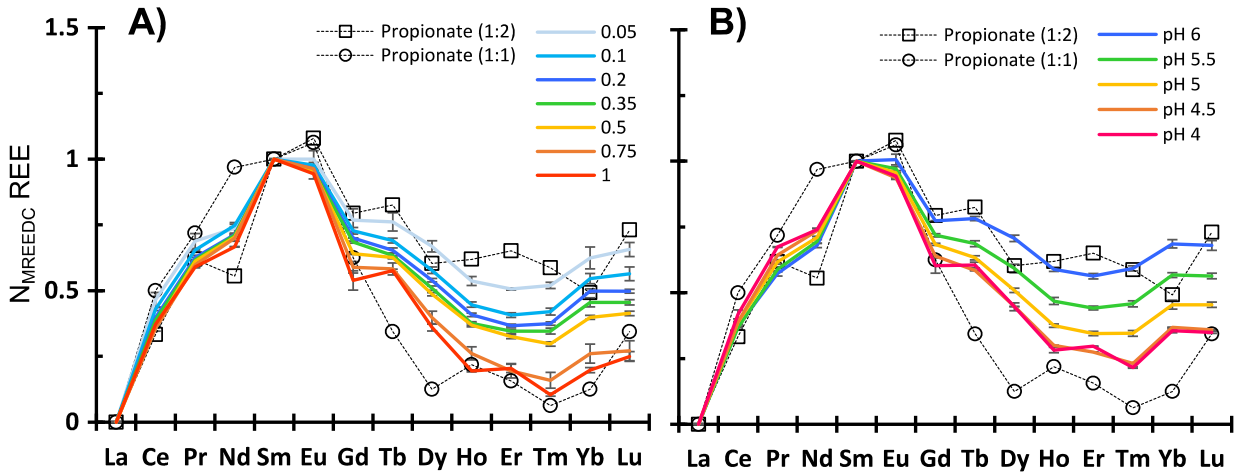

Figure 7. Comparison of REE-e-NPs patterns normalized to the MREE downward concavity A) relative to the REE/NPs ratios in mg g^{-1} C and B) relative to pH with the 1:1 and 1:3 REE-propionate complexes patterns normalized to the MREE downward concavity. Error bars correspond to the SD of the triplicates.

For the e-NPs, the N_{MREEDC} REE patterns showed a decrease with the increasing REE/NPs ratios (Figure 7A), highlighting the complexes' denticity evolution. These REE pattern variations showed that bi-ligand complexes were formed at low REE/NPs ratios (low loading). In contrast, they formed mono-ligands complexes at high REE/NPs ratios (high loading), as previously observed by Marsac et al.(34) for humic acid. Between pH 5 and 6, REE pattern variations demonstrated that more bi-ligand complexes occurred in coherence with the increasing number of ionized sites at the e-NPs. However, the N_{MREEDC} REE patterns did not evolve between pH 4 and 4.5, suggesting that bi-ligand complexes' contribution was insignificant under pH 4.

To summarize, REE adsorption onto NPs is driven by their binding to carboxylic sites present or developed at the NPs surface (Figure 2, 3, 6 and 7). The REE pattern variations could be attributed to the complex denticity. A MREE downward concavity was developed for all REE patterns, excluding

View Article Online
DOI: 10.1039/D2EN00048B

the formation of chelate complexes at the NPs surface. Rare earth elements are bound as REE-COOH mono and bi-ligand complexes. The low site density of the PSL free combined with the resulting intense competition with Y, U, Sc, and Th, highlight that LREE forms a weaker mono-ligand complex while HREE forms stronger bi-ligand complexes. The mono-ligand complexes dominated all REE at high REE/NPs and low pH (low availability of the binding sites). In contrast, the bi-ligand complexes dominated HREE at low REE/NPs and high pH (high availability of the binding sites). These results are in concordance with Marsac et al. (34,40,44,45) for REE binding with humic acid.

Implications for environmental NPs behavior

The present result demonstrates that REEs are bound onto the NPs surface via COOH groups. These surface sites are present onto PSLs because of their production protocol and onto e-NPs by their degradation route (photo-oxidation) under environmental conditions (24). The REE binding to NPs appeared strongly dependent on pH. The natural water pH is ranged from 6 to 9 (46,47) and the pKa of the COOH group varies between 4 and 5.5 (48). Therefore, COOH groups are deprotonated and strongly available for metal binding under natural conditions. The REE complexes formed at the surface of e-NPs could vary between monodentate and bidentate complexes relative to the REE and the REE/e-NPs ratio and pH. For pH>4.5 and low REE/e-NPs ratio, as under environmental conditions, REE are mainly bound to e-NPs as bi-ligands complexes, notably HREE. The stability constant of bi-ligands complexes is higher than mono-ligand complexes indicating that e-NPs can strongly adsorb REE and mainly HREE from the environment. Contrary to the formation of bi-ligands, results showed that chelate could not be formed on the e-NPs surface with REE, probably due to geometric constraints (low flexibility of the e-NPs structure, distances between –COOH groups) and site density. Therefore, it can be extrapolated that REEs act as cationic bridges between 2 e-NPs and thus influence the homo-aggregation of e-NPs (Figure 8) at high pH and REE/e-NPs ratios. Further study has to be performed to confirm such aggregation that can confirm the presence of bi-ligands complexes.

View Article Online
DOI: 10.1039/D2EN00048B

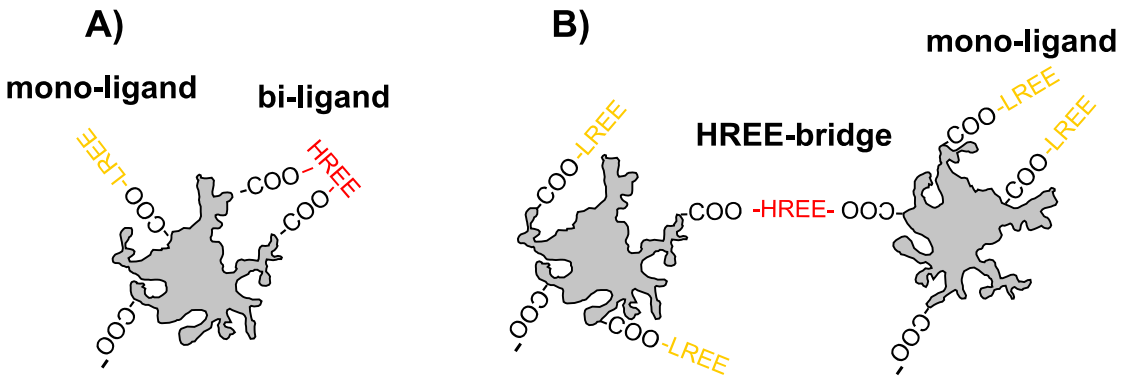

Figure 8. Possible complexes formed between LREE, HREE, and e-NPs, A) simple HREE Bi-ligand complex onto 1 e-NPs and B) HREE bi-ligand complex between 2 e-NPs acting as a cationic bridge and potentially resulting in e-NPs homo-aggregation.

Moreover, once adsorbed onto e-NPs, REE (and more generally metals) can penetrate living organisms. The prevailing pH conditions and as previously observed for $PSL_{surfactant}$ (49), can be released into the living organisms following a Trojan horse effect. However, this release will be controlled by the strength of the complexes. For REE, the present results clearly show that LREE (domination of mono-ligands complexes) will be more released than HREE (bi-ligands complexes).

Conclusions

Rare-earth element adsorption experiments were carried out to investigate trace metal-NPs interactions. For the studied NPs models, an MREE downward concavity was developed on the REE-NPs binding patterns corresponding to the sorption of REE onto -COOH groups. Under environmental conditions, –COOH sites are produced in response to the photo-oxidation of the plastics debris. A detailed study of the adsorption isotherm and REE patterns variations with the REE/NPs ratios and pH combined to the competition between REE and other ions demonstrated that LREE were mainly bound as mono-ligands complexes. At the same time, HREE specifically formed bi-ligands complexes with NPs. The binding sites' availability influences the proportion of mono and bi-ligands, influenced by the pH and the REE/NPS ratio. Under environmental conditions (pH >4.5 and low REE concentrations), bi-ligands complexes are thus expected to be dominant, notably for HREE. These results provide exciting

View Article Online
DOI: 10.1039/D2EN00048B

information and constraint, valuable for further investigations, notably the thermodynamic modelling of metal-NPs binding mechanisms.

Acknowledgments

This work was supported by the PEPSEA and PLASTISCARE project funded by ANR (project number ANR-17-CE34-0008 et ANR-19-CE04-0007). Through the GeOHeLiS analytical platform of Rennes 1 University, this work was also supported by the European Union via the European Regional Development Fund (FEDER), the French ministry of Higher Education and Research, the French Region of Brittany and Rennes Metropole. We acknowledge the Ocean Clean up foundation for their plastics debris donation namely, Boyan Slat, Laurent Lebreton, Fatimah Sulu Gambari, Matthias Egger and Gerianne Terlouw.

View Article Online
DOI: 10.1039/D2EN00048B

References

1. Ter Halle A, Jeanneau L, Martignac M, Jardé E, Pedrono B, Brach L, et al. Nanoplastic in the North Atlantic Subtropical Gyre. Environmental Science & Technology. 5 déc 2017;51(23):13689‑97.

2. Materić D, Kasper-Giebl A, Kau D, Anten M, Greilinger M, Ludewig E, et al. Micro- and Nanoplastics in Alpine Snow: A New Method for Chemical Identification and (Semi)Quantification in the Nanogram Range. Environ Sci Technol. 18 févr 2020;54(4):2353‑9.

3. Wahl A, Le Juge C, Davranche M, El Hadri H, Grassl B, Reynaud S, et al. Nanoplastic occurrence in a soil amended with plastic debris. Chemosphere. janv 2021;262:127784.

4. Lambert S, Sinclair CJ, Bradley EL, Boxall ABA. Effects of environmental conditions on latex degradation in aquatic systems. Science of The Total Environment. mars 2013;447:225‑34.

5. da Costa JP, Santos PSM, Duarte AC, Rocha-Santos T. (Nano)plastics in the environment – Sources, fates and effects. Science of The Total Environment. oct 2016;566‑567:15‑26.

6. Dawson AL, Kawaguchi S, King CK, Townsend KA, King R, Huston WM, et al. Turning microplastics into nanoplastics through digestive fragmentation by Antarctic krill. Nature Communications [Internet]. déc 2018 [cité 22 mai 2019];9(1). Disponible sur: http://www.nature.com/articles/s41467-018-03465-9

7. Mattsson K, Jocic S, Doverbratt I, Hansson L-A. Nanoplastics in the Aquatic Environment. In: Microplastic Contamination in Aquatic Environments [Internet]. Elsevier; 2018 [cité 20 déc 2018]. p. 379‑99. Disponible sur: https://linkinghub.elsevier.com/retrieve/pii/B9780128137475000138

8. Gigault J, Halle A ter, Baudrimont M, Pascal P-Y, Gauffre F, Phi T-L, et al. Current opinion: What is a nanoplastic? Environmental Pollution. avr 2018;235:1030‑4.

9. Orts-Gil G, Natte K, Österle W. Multi-parametric reference nanomaterials for toxicology: state of the art, future challenges and potential candidates. RSC Adv. 2013;3(40):18202.

10. Davranche M, Veclin C, Pierson-Wickmann A-C, El Hadri H, Grassl B, Rowenczyk L, et al. Are nanoplastics able to bind significant amount of metals? The lead example. Environmental Pollution. juin 2019;249:940‑8.

11. Yu F, Yang C, Zhu Z, Bai X, Ma J. Adsorption behavior of organic pollutants and metals on micro/nanoplastics in the aquatic environment. Science of The Total Environment. déc 2019;694:133643.

12. Gigault J, El Hadri H, Nguyen B, Grassl B, Rowenczyk L, Tufenkji N, et al. Nanoplastics are neither microplastics nor engineered nanoparticles. Nat Nanotechnol. mai 2021;16(5):501‑7.

13. Chen Q, Yin D, Jia Y, Schiwy S, Legradi J, Yang S, et al. Enhanced uptake of BPA in the presence of nanoplastics can lead to neurotoxic effects in adult zebrafish. Science of The Total Environment. déc 2017;609:1312‑21.

14. Rist S, Hartmann NB. Aquatic Ecotoxicity of Microplastics and Nanoplastics: Lessons Learned from Engineered Nanomaterials. In: Wagner M, Lambert S, éditeurs. Freshwater Microplastics [Internet]. Cham: Springer International Publishing; 2018 [cité 5 août 2021]. p. 25‑49. (The Handbook of Environmental Chemistry; vol. 58). Disponible sur: http://link.springer.com/10.1007/978-3-319-61615-5_2

15. Baudrimont M, Arini A, Guégan C, Venel Z, Gigault J, Pedrono B, et al. Ecotoxicity of polyethylene nanoplastics from the North Atlantic oceanic gyre on freshwater and marine organisms (microalgae and filter-feeding bivalves). Environ Sci Pollut Res. févr 2020;27(4):3746‑55.

16. Flick EW. Plastics Additives, Volume 1: An Industry Guide. Elsevier; 2013. 313 p.

View Article Online
DOI: 10.1039/D2EN00048B

17. Piringer OG, Baner AL. Plastic Packaging: Interactions with Food and Pharmaceuticals. John Wiley & Sons; 2008. 635 p.

18. Turner A, Filella M. Hazardous metal additives in plastics and their environmental impacts. Environment International. 1 nov 2021;156:106622.

19. Town RM, van Leeuwen HP, Blust R. Biochemodynamic Features of Metal Ions Bound by Micro- and Nano-Plastics in Aquatic Media. Frontiers in Chemistry. 2018;6:627.

20. Catrouillet C, Davranche M, Khatib I, Fauny C, Wahl A, Gigault J. Metals in microplastics: determining which are additive, adsorbed, and bioavailable. Environmental Science: Processes & Impacts. 2021;23(4):553‑8.

21. Kalogerakis N, Karkanorachaki K, Kalogerakis GC, Triantafyllidi EI, Gotsis AD, Partsinevelos P, et al. Microplastics Generation: Onset of Fragmentation of Polyethylene Films in Marine Environment Mesocosms. Frontiers in Marine Science [Internet]. 28 mars 2017 [cité 22 mai 2019];4. Disponible sur: http://journal.frontiersin.org/article/10.3389/fmars.2017.00084/full

22. Wang J, Peng J, Tan Z, Gao Y, Zhan Z, Chen Q, et al. Microplastics in the surface sediments from the Beijiang River littoral zone: Composition, abundance, surface textures and interaction with heavy metals. Chemosphere. mars 2017;171:248‑58.

23. Wang Q, Zhang Y, Wangjin X, Wang Y, Meng G, Chen Y. The adsorption behavior of metals in aqueous solution by microplastics effected by UV radiation. Journal of Environmental Sciences. janv 2020;87:272‑80.

24. Blancho F, Davranche M, Fumagalli F-S, Ceccone G, Gigault J. A reliable procedure to obtain environmentally relevant nanoplastics proxies. Environ Sci: Nano. 2021;10.1039.D1EN00395J.

25. Tang S, Lin L, Wang X, Yu A, Sun X. Interfacial interactions between collected nylon microplastics and three divalent metal ions (Cu(II), Ni(II), Zn(II)) in aqueous solutions. Journal of Hazardous Materials. févr 2021;403:123548.

26. Bargar JR, Brown GE, Parks GA. Surface complexation of Pb(II) at oxide-water interfaces: I. XAFS and bond-valence determination of mononuclear and polynuclear Pb(II) sorption products on aluminum oxides. Geochimica et Cosmochimica Acta. juill 1997;61(13):2617‑37.

27. Ponthieu M, Juillot F, Hiemstra T, van Riemsdijk WH, Benedetti MF. Metal ion binding to iron oxides. Geochimica et Cosmochimica Acta. juin 2006;70(11):2679‑98.

28. Fitts JP, Trainor TP, Grolimund D, Bargar JR, Parks GA, Brown GE. Grazing-incidence XAFS investigations of Cu(II) sorption products at α-Al_2O_3–water and α-SiO_2–water interfaces. J Synchrotron Rad. 1 mai 1999;6(3):627‑9.

29. Sverjensky DA. Prediction of the speciation of alkaline earths adsorbed on mineral surfaces in salt solutions. Geochimica et Cosmochimica Acta. mai 2006;70(10):2427‑53.

30. Yano J, Yachandra VK. X-ray absorption spectroscopy. Photosynth Res. déc 2009;102(2‑3):241‑54.

31. de Baar HJW, Schijf J, Byrne RH. Solution chemistry of the rare earth elements in seawater. European Journal of Solid State and Inorganic Chemistry,. 1991;(28(Suppl)):357‑73.

32. McLennan SM. Rare earth element geochemistry and the “tetrad” effect. Geochimica et Cosmochimica Acta. mai 1994;58(9):2025‑33.

33. Pourret O, Davranche M, Gruau G, Dia A. Rare earth elements complexation with humic acid. Chemical Geology. août 2007;243(1‑2):128‑41.

34. Marsac R, Davranche M, Gruau G, Dia A. Metal loading effect on rare earth element binding to humic acid: Experimental and modelling evidence. Geochimica et Cosmochimica Acta. mars 2010;74(6):1749‑61.

View Article Online
DOI: 10.1039/D2EN00048B

35. Davranche M, Grybos M, Gruau G, Pédrot M, Dia A, Marsac R. Rare earth element patterns: A tool for identifying trace metal sources during wetland soil reduction. Chemical Geology. mai 2011;284(1‑2):127‑37.

36. Noack CW, Dzombak DA, Karamalidis AK. Rare Earth Element Distributions and Trends in Natural Waters with a Focus on Groundwater. Environ Sci Technol. 15 avr 2014;48(8):4317‑26.

37. Taylor SR, McLennan SM. Chapter 79 The significance of the rare earths in geochemistry and cosmochemistry. In: Handbook on the Physics and Chemistry of Rare Earths [Internet]. Elsevier; 1988 [cité 23 sept 2021]. p. 485‑578. Disponible sur: https://linkinghub.elsevier.com/retrieve/pii/S0168127388110118

38. Wood SA. The aqueous geochemistry of the rare-earth elements: Critical stability constants for complexes with simple carboxylic acids at 25°C and 1 bar and their application to nuclear waste management. Engineering Geology. sept 1993;34(3‑4):229‑59.

39. Byrne RH, Li B. Comparative complexation behavior of the rare earths. Geochimica et Cosmochimica Acta. 1 nov 1995;59(22):4575‑89.

40. Marsac R, Davranche M, Gruau G, Bouhnik-Le Coz M, Dia A. An improved description of the interactions between rare earth elements and humic acids by modeling: PHREEQC-Model VI coupling. Geochimica et Cosmochimica Acta. oct 2011;75(19):5625‑37.

41. Pessoni L, Veclin C, El Hadri H, Cugnet C, Davranche M, Pierson-Wickmann A-C, et al. Soap- and metal-free polystyrene latex particles as a nanoplastic model. Environ Sci: Nano. 2019;6(7):2253‑8.

42. Davranche M, Pourret O, Gruau G, Dia A, Le Coz-Bouhnik M. Adsorption of REE(III)-humate complexes onto MnO2: Experimental evidence for cerium anomaly and lanthanide tetrad effect suppression. Geochimica et Cosmochimica Acta. oct 2005;69(20):4825‑35.

43. Tang J, Johannesson KH. Speciation of rare earth elements in natural terrestrial waters: assessing the role of dissolved organic matter from the modeling approach. Geochimica et Cosmochimica Acta. juill 2003;67(13):2321‑39.

44. Marsac R, Davranche M, Gruau G, Dia A, Bouhnik-Le Coz M. Aluminium competitive effect on rare earth elements binding to humic acid. Geochimica et Cosmochimica Acta. 15 juill 2012;89:1‑9.

45. Marsac R, Davranche M, Gruau G, Dia A, Pédrot M, Le Coz-Bouhnik M, et al. Effects of Fe competition on REE binding to humic acid: Origin of REE pattern variability in organic waters. Chemical Geology. 29 mars 2013;342:119‑27.

46. Mattson MD. Acid lakes and rivers. In: Environmental Geology [Internet]. Dordrecht: Kluwer Academic Publishers; 1999 [cité 15 juin 2021]. p. 6‑9. (Encyclopedia of Earth Science). Disponible sur: http://link.springer.com/10.1007/1-4020-4494-1_4

47. Jiang L-Q, Carter BR, Feely RA, Lauvset SK, Olsen A. Surface ocean pH and buffer capacity: past, present and future. Sci Rep. déc 2019;9(1):18624.

48. Martell AE, Smith RM. Other Organic Ligands [Internet]. Boston, MA: Springer US; 1977 [cité 23 févr 2021]. Disponible sur: http://link.springer.com/10.1007/978-1-4757-1568-2

49. Abdolahpur Monikh F, Chupani L, Vijver MG, Peijnenburg WJGM. Parental and trophic transfer of nanoscale plastic debris in an assembled aquatic food chain as a function of particle size. Environmental Pollution. janv 2021;269:116066.